Journal of
Materials Chemistry A

Accepted Manuscript

This article can be cited before page numbers have been issued, to do this please use: L. Deng, W. Zhong, J. Chen, P. Zhang, X. Ren, Y. Li, H. Mi, L. Yao and L. Sun, *J. Mater. Chem. A*, 2017, DOI: 10.1039/C7TA05035F.

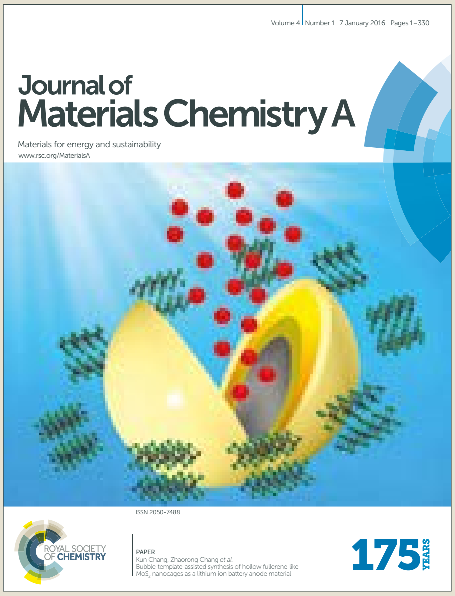

ROYAL SOCIETY OF CHEMISTRY

View Article Online
DOI: 10.1039/C7TA05035F

Journal of Materials Chemistry A

COMMUNICATION

Air plasma etching towards rich active sites in Fe/N-porous carbon for oxygen reduction reaction with superior catalytic performance

Received 00th January 20xx,
Accepted 00th January 20xx

DOI: 10.1039/x0xx00000x

www.rsc.org/

Wenhua Zhong[a], Jiaxiang Chen[a], Peixin Zhang*[a,b], Libo Deng*[a], Lei Yao[a], Xiangzhong Ren[a], Yongliang Li[a], Hongwei Mi[a] and Lingna Sun[a]

Herein, an electrocatalyst consisting of iron and nitrogen co-doped porous carbon (Fe-N/C) was prepared by catalytic carbonization of chitin with the assistance of $FeCl_3$ and $ZnCl_2$. The catalytic activity of Fe-N/C towards oxygen reduction reaction (ORR) in both acidic and alkaline electrolytes was significantly enhanced by air-plasma etching for only 120 s, showing a four-electron ORR process with onset potential and limiting current comparable to Pt catalyst. This performance enhancement was originated from the removal of less stable sp^3 and amorphous sp^2 carbons which would expose more active catalytic center FeN_4, as well as the transformation of a small fraction of iron-based nanoparticles into FeN_4 species.

Platinum-loaded carbons (Pt/C) have long been considered as the benchmark electrocatalysts for cathodic oxygen reduction reaction (ORR) which is a rate-controlling step in fuel cells and metal-air batteries.[1-3] However, the high cost, poor durability, and intolerance to fuel crossover for Pt-based catalysts have hindered the widespread application of these energy-conversion devices. It is thus vital to develop cost-effective electrocatalysts with high performance to replace Pt-based catalysts. Recently, iron and nitrogen co-doped carbon (Fe-N/C) has been receiving tremendous interests due to their high ORR activity, particularly due to their advantages over other non-Pt electrocatalysts in acidic media.[4-7]

The catalytic efficiency relies heavily on the diffusion and contact of oxygen with the catalytic centres as well as the electron transfer within the catalysts and across the electrolyte-catalyst interface. Particularly, it has been demonstrated recently that active catalytic sites mainly form at the edges of graphitic sheets, which exist predominantly in micropores.[8-10] As such, open structures that allow readily access of reactants to the catalytic centres is crucial for efficient ORR process. Traditional methods of preparing Fe-N/C electrocatalysts usually involve pyrolysis of precursors consisting of Fe, N and C elements at high temperatures. Only a small fraction of the active sites are exposed while the rests are embedded in the matrix of Fe-N/C and thus poor performance is obtained in the pyrolyzed carbons.[11-13] To address this issue, numerous methods have been developed, such as using the versatile matrix material graphene to load active centers and controlling the pore structure of catalysts using template synthesis.[11, 14, 15] However, most of those methods are tedious, costly and difficult to scale up.

Herein, we report a facile method to enhance the electrocatalytic performance of an Fe-N/C electrocatalyst through plasma etching. Chitin which is the second most abundant and nitrogen-rich biopolymer was used as the precursor to prepare the carbon matrix. To obtain a high

---

[a] *College of Chemistry and Environmental Engineering, Shenzhen University, Shenzhen 518060, China.*
[b] *Shenzhen Key Laboratory of Environmental Chemistry and Ecological Remediation, Shenzhen University, Shenzhen 518060, P. R. China.*

Electronic Supplementary Information (ESI) available: [Experimental details, strutural charactierizations and electrochemical performances of the catalysts]. See DOI: 10.1039/x0xx00000x

View Article Online
DOI: 10.1039/C7TA05035F

surface area and a high degree of graphitization simultaneously, the precursor was carbonized with the assistance of both $FeCl_3$ and $ZnCl_2$, which resulted in Fe and N co-doped porous carbon after acid leaching. The sample was further etched by air plasma which exposes the catalytic active Fe-N (pyridinic N) species, through which excellent catalytic performances towards ORR in both acidic and alkaline media were obtained.

The precursor was first pre-oxidized in air and impregnated with $FeCl_3$ and $ZnCl_2$ prior to the high-temperature treatment. Coordination of Fe and Zn with the polar groups of chitin enables a high capacity for adsorption of $FeCl_3$ and $ZnCl_2$ by chitin, which facilitates the catalytic graphitization and creation of porous structure upon carbonization at 800 °C (Experimental details are described in the electronic supplementary information (ESI)). The subsequent acid leaching removed most of the metal compounds on the surface, leaving a low content of nanoparticles which were encapsulated tightly in the carbon matrix, as can be seen from the transmission electron microscopy (TEM) image shown in Fig. 1a. High resolution TEM (HRTEM) images revealed the carbon is partially graphitized with a low structural order, and the average diameter of the nanoparticles is ~7 nm (Fig. 1b). Elemental mapping through X-ray energy dispersive spectroscopy (EDS) suggests the uniform distribution of carbon, oxygen and nitrogen in the pyrolyzed carbon (Fig. S1 in the supporting information) and the nanoparticles shown in Fig. 1c are mainly consisted of iron, oxygen and nitrogen (Fig. 1d). The Fe species that survived after acid leaching are uniformly distributed in the carbon/nitrogen matrix, which are believed to contribute to highly active FeN_4 active sites. However, most of the active sites are embedded in the matrix of Fe-N/C, which are not easily accessible for the reactants, which is reflected by a low electrocatalytic performance. Re-annealing the acid-leached Fe-N/C at 800 °C did not improve the catalytic performance as significant as Dodelet showed.[16] Thus air-plasma treatment was applied to tune the surface properties of the electrocatalyst (the samples were denoted as Fe-N/C-*x*, where *x* refers to the plasma treatment time). Scanning electron microscopy images illustrated that the surface of as-prepared carbon monolith before plasma etching is intact and smooth (Fig. 1e). After treating by air plasma for 120 s (i.e. Fe-N/C-120), the surface becomes rougher and ordered trenches can be clearly seen from Fig. 1f (SEM images for samples treated for different durations are shown in Fig. S2). HRTEM images for Fe-N/C-120 (Fig. S3) suggested that more defects are created upon plasma etching, which is consistent with SEM observation. It is also noted the content of iron-containing nanoparticles is decreased after plasma etching.

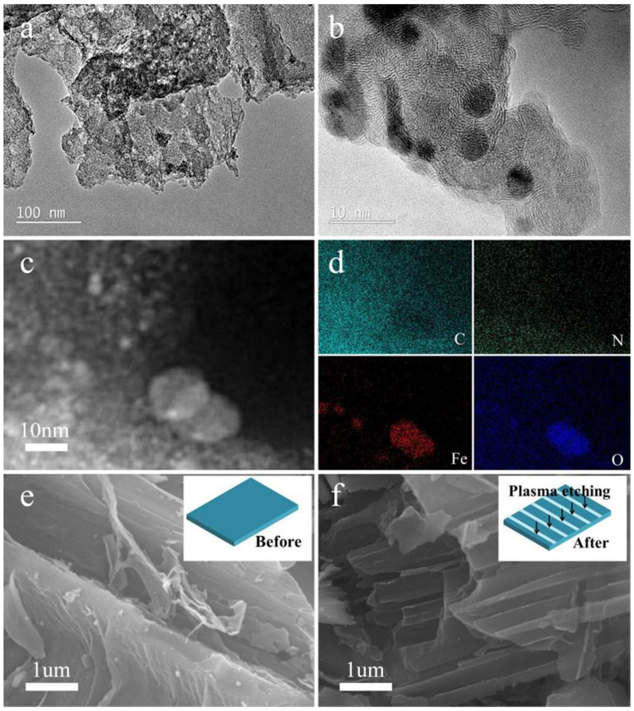

Fig. 1 (a), (b) and (c): TEM images of Fe-N/C catalyst and (d) EDS elemental mapping corresponding to the area in (c); SEM images for (e) Fe-N/C-0 and (f) Fe-N/C-120.

Plasma etching also induced changes in other aspects: (1) XRD characterization (Fig. 2a) showed that the as-pyrolyzed carbon is crystalline (strong reflection at 26°) which endows a high conductivity to the carbon. Upon plasma etching, the crystallinity further increased slightly due to removal of less stable sp^3 carbon and amorphous sp^2 carbon; (2) Raman spectroscopy tests disclosed that the D-band (at ~1340 cm^{-1})

View Article Online
DOI: 10.1039/C7TA05035F

becomes stronger relative to the G-band (at ~1586 cm^{-1}) as the irradiation time increases to 120 s but becomes slightly weaker as the etching time is extended (Fig. 2b), suggesting that more defects were created upon plasma etching, which agrees well with the TEM observation shown in Fig. S3. We speculate that topological defects such as carbon vacancies, Stone-Wales defects, edges of planes and open ends are introduced to the Fe-N/C catalysts after the air plasma etching.[17, 18] (3) Fourier transform infrared (FTIR) spectra showed that the concentration of hydrophilic groups in the Fe-N/C-0 such as the absorption at 3433 cm^{-1} corresponding to OH group is obviously enhanced upon plasma etching (Fig. 2c); (4) The Brunauer–Emmett–Teller (BET, Fig. 2d) surface area increased from 1730 m^2 g^{-1} for Fe-N/C-0 to 1963 m^2 g^{-1} for Fe-N/C-120 but decreased to 1780 m^2 g^{-1} for Fe-N/C-240, and the corresponding pore volume (Fig. S4) also increased slightly from 0.92 cm^3 g^{-1} to 1.05 cm^3 g^{-1} as determined by nitrogen adsorption/desorption measurements. Moreover, the rich micropores as disclosed by the adsorption/desorption isotherms in these catalysts are crucial for catalytic activity due to that it is the micropore that mainly hosts the catalytic active centers in N-doped carbons.[9]

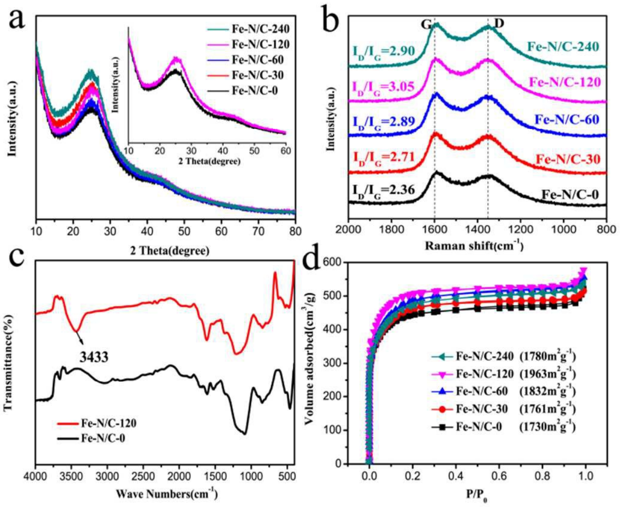

Fig. 2 Characterization of the effects of plasma etching on structure of Fe-N/C: (a) XRD patterns, (b) Raman spectra, (c) FT-IR spectra, and (d) N_2 adsorption-desorption curves for the Fe-N/C electrocatalysts.

X-ray photoelectron spectroscopy (XPS) measurements were performed to further analyze the change of composition and chemical state upon plasma etching. The full spectra are shown in Fig. S5 and the compositions are listed in Table S1. It is noted the content of oxygen increased significantly after treating with plasma, from 11.43at% for Fe-N/C-0 to 22.00at% for Fe-N/C-120 but decreased slightly to 19.7% by further extending the etching time to 240 s (Fig. S6). The increase of oxygen content would increase the hydrophilicity of the carbon matrix, facilitate the diffusion and bonding of oxygen with the carbon surface and consequently improve the catalytic efficiency.[19] In the meanwhile, the content of carbon dropped steadily due to the loss of less stable sp^3 and amorphous sp^2 carbons (Fig. S6).

In the high resolution Fe 2p XPS spectrum of Fe-N/C-0, the peaks at 711.0 and 724.3eV (Fig. S7) were assigned to Fe $2p_{3/2}$ and Fe $2p_{1/2}$, respectively, suggesting the existence of iron oxides. The atomic content of Fe was 0.84% for Fe-N/C-0 and remained almost constant (within experimental error) after plasma etching.

The high-resolution N1s spectra of all Fe-N/C catalysts can be deconvoluted into three peaks with binding energies of 398.6, 400.1, and 401.0 eV, corresponding to pyridinic N, pyrrolic N, and graphitic N, respectively (Fig. 3a). The peak at 398.6 eV also includes the contribution from nitrogen bound to iron (Fe-N) due to the small difference between binding energies of Fe-N and pyridinic N.[11, 20] The central Fe ion would coordinate with four pyridinic N that are located at the edges of graphitic domains. The total nitrogen species accounted for 7.15at% in Fe-N/C-0 which is remarkably higher than those obtained by direct pyrolysis or by $ZnCl_2$ activation of chitin.[21, 22] Such a high doping level is attributed to the coordination between N and Fe which would prevent the evaporation of N species during pyrolysis. The total content of nitrogen species only varied slightly upon irradiation to plasma. However, the relative composition of N species changed significantly, i.e. the fraction of pyridinic N (including Fe-N) increased steadily with the increase of etching time, from 20.0% for Fe-N/C-0 to 28.8% for Fe-N/C-120 (Fig. 3b) whereas the pyrrolic N decreased from 48.3% to 37.5%. It is now generally recognized that the Fe-N

View Article Online
DOI: 10.1039/C7TA05035F

(pyridinic N) are the catalytic active centers for ORR. Hence, the increase of these nitrogen species might enhance the catalytic performance which will be discussed later.

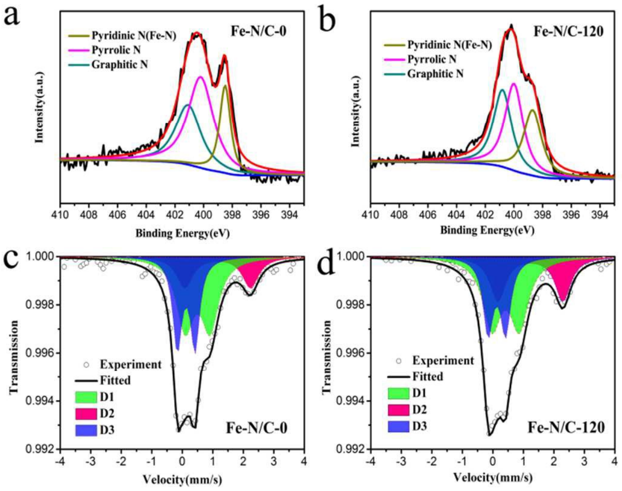

Fig. 3 (a-b) XPS spectra and (c-d) Mössbauer absorption spectra for Fe-N/C-0 and Fe-N/C-120.

The chemical state of iron in the Fe-N-C was further characterized using ^{57}Fe Mössbauer spectroscopy (Fig. 3c). The Mössbauer parameters of each component are shown in Table S2. Three doublets (D1, D2 and D3) with unique isomer shift (δ_{iso}) and quadrupole splitting (ΔE_{Q}), which correspond to $\text{Fe}^{2+}/\text{Fe}^{3+}$ species are clearly identified. No elemental Fe (i.e. singlet peak) was detected from the spectrum for Fe-N/C-0. D1 with an δ_{iso} of 0.42 mm s^{-1} and ΔE_{Q} of 0.9 mm s^{-1} is assigned to a four-fold nitrogen coordination of Fe^{II} in low-spin ($\text{Fe}^{\text{II}}\text{N}_4$, LS), and would contribute to the catalytic performance in acid electrolytes.[23, 24] However, a recent study showed that the doublet D2 which has an δ_{iso} of 1.23 mm s^{-1} and ΔE_{Q} of 2.13 mm s^{-1} and is associated with high-spin $\text{Fe}^{\text{II}}\text{N}_4$, is the most active site for ORR.[16, 25, 26] The doublet D3 is related to surface-oxidized and nitrogen-rich iron nanoparticles and is less catalytic active.[27] It is noted that after treating with plasma for 120 s, the fraction of D1 among the total iron species remains almost constant whereas the D2 component increases significantly with the expense of D3 (Fig. 3d). This change might be due to the sputtering of Fe atoms from the nanoparticles by plasma, which would migrate into the adjacent micropore to coordinate with the pyridinic N at the edges of graphitic domains. This change is also consistent with the increase of pyridinic N revealed by XPS, which confirmed that more active sites are exposed upon plasma etching.

Such modifications in chemical state and microstructure of Fe-N/C induced by plasma etching might pose profound effects on its electrocatalytic activity. The performance of these catalysts in an acid electrolyte HClO_4 (0.1 M) was first assessed by cyclic voltammetry (CV) and the curves are shown in Fig. S8a. A single cathodic peak resulting from O_2 reduction can be seen in the O_2-saturated electrolyte whereas no such reduction peak was observed when the electrolyte was N_2-saturated. With the increase of plasma etching time, the ORR peak becomes stronger and the peak potential shifted positively to 0.694 V at 120 s (Fig. S8b). These results clearly suggest that the catalytic activity is enhanced by plasma etching. However, extending the etching time to 240 s degraded to performance slightly compared to the one etched for 120 s, due possibly to the slight but noticeable drop of the surface area, the lower density of defects and the lower content of oxygen, which are in turn due possibly to collapse of micropores, over-etching of the crystalline carbon and evaporation of less stable oxygen-containing groups. It is shown later that the change of these structural parameters is in excellent agreement with the performance order among our plasma-etched Fe-N/C catalysts. The optimal etching time is 120 s in this case.

The electrocatalytic activity was further evaluated from linear-sweep voltammetry (LSV) performed on a rotating disk electrode (RDE) at the same catalyst loading (0.14mg cm^{-2}). The onset potential (determined as the potential at 5% of the limiting diffusion current from the LSV curve[28]) also shifted positively with the increase of plasma etching time, which was found to be 0.745 V, 0.746 V, 0.750 V, and 0.812 V for Fe-N/C-0, Fe-N/C-30, Fe-N/C-60, and Fe-N/C-120 (Fig. 4a), respectively. It should be noted that even better performances can be obtained for these materials when higher loadings of catalysts

View Article Online
DOI: 10.1039/C7TA05035F

on the electrode are used for testing. The onset potential for Fe-N/C-120 at a loading of 0.60mg cm^{-2} was 0.88 V which is close to that of the commercial Pt/C and comparable with the leading results reported in literatures for Fe- and Co- doped carbons in an acidic electrolyte, (Table S3).[13, 29, 30] The current density for these catalysts also exhibited a similar order, i.e. the current at 0.3 V ($J_{0.30}$) increased from 1.96 mA cm^{-2} for Fe-N/C-0 to 3.56 mA cm^{-2} for Fe-N/C-120 (parameters listed Table S4) and the limiting current increased from 2.55 mA cm^{-2} to 3.86 mA cm^{-2}. Furthermore, the electron transfer number (n) determined at 0.3 V using the Koutecky–Levich (K–L) equations (Eqs. S1-S3 in) increased from 2.73 for Fe-N/C-0 to 3.18, 3.55, and 3.77 for Fe-N/C-30, Fe-N/C-60, and Fe-N/C-120, respectively (Fig. 4b and Fig. S9). These results suggest that the ORR occurs on the as-prepared Fe-N-C catalysts through a combination of two-electron and four-electron processes. After etching with air plasma for 120s, the catalysts can promote the ORR predominately through a four-electron pathway. These results thus confirmed that an outstanding catalytic performance can be achieved through plasma etching for just 120 s.

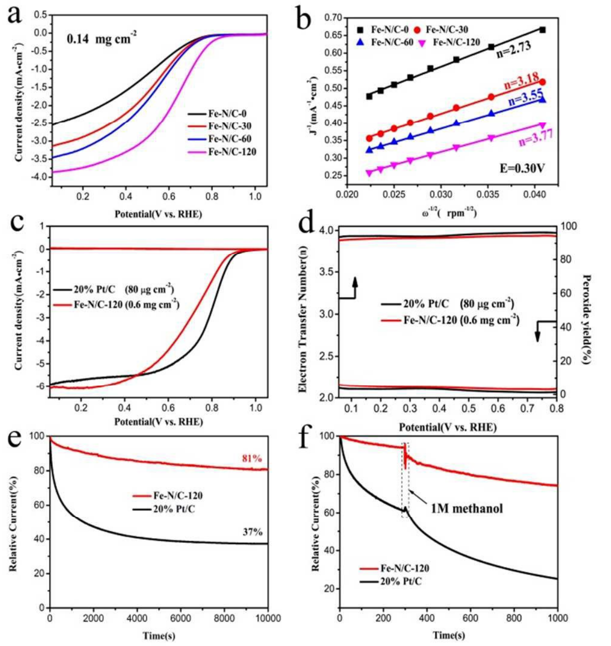

Fig. 4 Electrocatalytic performance evaluation for the electrocatalysts: (a) LSV curves (loading ~0.14 mg cm^{-2}, scan rate 10 mV s^{-1} and rotating rate 1600 rpm), (b) K-L plots , (c) LSV curves measured using an RRDE for Fe-N/C-120 (loading ~0.6 mg cm^{-2}) and Pt/C (loading ~80 μg cm^{-2}), (d) the H_2O_2 yields as a function of potential, (e) Durability evaluation at 0.3 V and a rotation rate of 1600 rpm for Pt/C and (f) Chronoamperometric responses on addition of 1M methanol after about 300 s.

To gain further insight into the ORR on the catalysts, the catalytic efficiency was also analysed using rotating-ring disk electrode (RRDE, Fig. 4c). The corresponding ring current was simultaneously measured with a Pt ring electrode for detecting peroxide species formed at the disk electrode. The n values and the corresponding H_2O_2 yield can be also determined from the disk and ring currents using Eq. S4 and Eq. S5, respectively. It was found that in the potential range of 0.2 V to 0.8 V, the n values for Fe-N/C-120 are in the range of 3.90-3.93 (Fig. 4d). The trend of the n value calculated from RRDE tests are in good agreement with those determined from the K-L plots (Fig. S9). The corresponding H_2O_2 yields on Fe-N/C-120 were found to be 4.71-3.40%, which is comparable with that of 20% Pt/C (3.18-1.39%).

Long-term durability and tolerance to the methanol crossover effect are crucial for practical applications of electrocatalysts. The durability of Fe-N/C-120 and 20% Pt/C was evaluated by measuring the current loss after prolonged operation at a fixed potential in O_2-saturated 0.1 M $HClO_4$ solution for 10000 s (Fig. 4e). It can be seen that Fe-N/C-120 retained 81% of its initial current whereas the current retention for Pt/C is only 37% after continuous operation for 10000 s in 0.1 M $HClO_4$ solution, suggesting that the durability of Fe-N/C-120 is superior to the Pt/C catalyst in acid solution and suggests that the FeN_4 sites in the Fe–N/C catalyst are quite stable in an acidic environment.[5] To further assess the methanol-tolerance performance, 1 M methanol was introduced during the measurement of chronoamperometric response at 300s in 0.1 M $HClO_4$ solution (Fig. 4f). After the introduction of 1M methanol, only a slight disturbance in current density was observed for Fe-N/C-120, whereas an obvious reduction in current density was found for the Pt/C catalyst due to methanol oxidation. Therefore, Fe-N/C-120 exhibits excellent tolerance to methanol oxidation, which holds great promise for direct methanol fuel-cell technology.

View Article Online
DOI: 10.1039/C7TA05035F

As demonstrated above, plasma etching resulted in a higher content of FeN_4 and also led to a higher crystallinity, more defects, a higher content of oxygen-containing groups and a higher surface area in the Fe-N/C catalyst, all of which might improve the electrocatalytic performance. To get insight into the contribution of these aspects to the performance enhancement, the precursor chitin was activated by $ZnCl_2$ without using $FeCl_3$, and the activated carbon was also treated by air plasma and the electrocatalytic performance was evaluated (Fig. S10). Interestingly, the performance of the $ZnCl_2$-activated carbon after plasma etching was only improved slightly, with the limiting current increased from 0.79 mA cm^{-2} to 0.99 mA cm^{-2}, i.e. the catalytic performance is obviously inferior to that of the Fe-N/C. Moreover, the extent of performance enhancement upon plasma etching for the Fe-free carbon is also less pronounced than that for the Fe-N/C catalyst despite that plasma induced similar effects on structure of these carbons. Therefore, the performance enhancement is mainly attributed to the removal of sp^3 and amorphous sp^2 carbons which would expose the micropores that accommodate the highly active catalytic center FeN_4 (the proposed mechanism is shown in Fig. 5). Sputtering of iron atoms from the nanoparticles induced by plasma and the subsequent migration into micropores and creation of more high-spin Fe-N species would further improve the catalytic performance. In contrast, unblocking the micropores in Fe-free chitin-derived carbon by plasma is less efficient for performance improvement due to the lack of Fe-N species.

A parallel investigation of the performance for these catalysts in a KOH solution (0.1 M) disclosed similar behaviors, i.e. the as-prepared Fe-N/C without plasma etching showed a poor catalytic efficiency which was enhanced remarkably upon etching for 120s (Figs. S11-S13). Moreover, the performance in KOH is even better than in the acidic electrolyte. In the KOH solution, ORR occurs on Fe-N/C-120 through a four-electron process with an even higher *n* value ($n = 3.9$), the onset potential was 1.041 V and the limiting current was 6.29 mA cm^{-2} (loading ~0.6 mg cm^{-2}). These values are even superior to those for the benchmark Pt/C catalyst.

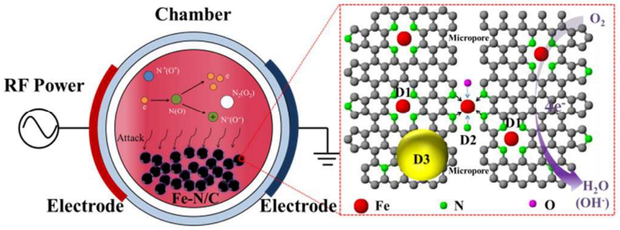

Fig. 5 A schematic diagram for the plasma etching process, the possible structure model for nitrogen species in Fe-N/C catalysts and the catalytic ORR process.

In summary, an Fe-N/C catalyst with excellent performances in both acidic and alkaline media has been prepared by treating chitin-derived carbon with air plasma for just 120 s. Structural characterizations suggested that the performance enhancement is associated with the removal of less stable carbons that exposes the active catalytic centers FeN_4, coupled with the transformation of iron-based nanoparticles into Fe-N species. The method of achieving high catalytic performances by plasma etching could extend to other materials and can be scaled up for mass production due to the fast processing and low cost, and would pave the way for practical applications of Fe-N/C catalysts.

This work was supported by the National Natural Science Foundation of China (Grants #51374146, 51602202), the Natural Science Foundation of Guangdong (2015A030310087), and Shenzhen Government's Plan of Science and Technology (Grants JCYJ20150324141711596 and JCYJ20160422112012739).

The authors declare no competing financial interests.

References

1 C. Zhu, H. Li, S. Fu, D. Du and Y. Lin, *Chem. Soc. Rev.*, 2016, **45**, 517-531.

2 Q. Jia, N. Ramaswamy, U. Tylus, K. Strickland, J. Li, A. Serov, K. Artyushkova, P. Atanassov, J. Anibal, C. Gumeci, S. C. Barton, M.-T. Sougrati, F. Jaouen, B. Halevi and S. Mukerjee, *Nano Energy*, 2016, **29**, 65-82.

3 L. T. Song, Z. Y. Wu, F. Zhou, H. W. Liang, Z. Y. Yu and S. H. Yu, *Small*, 2016, **12**, 6398-6406.

View Article Online
DOI: 10.1039/C7TA05035F

4 Y. Zhu, B. Zhang, X. Liu, D. W. Wang and D. S. Su, *Angew. Chem., Int. Ed.*, 2014, **53**, 10673-10677.

5 L. Lin, Q. Zhu and A. W. Xu, *J. Am. Chem. Soc.*, 2014, **136**, 11027-11033.

6 J.-C. Li, P.-X. Hou, C. Shi, S.-Y. Zhao, D.-M. Tang, M. Cheng, C. Liu and H.-M. Cheng, *Carbon*, 2016, **109**, 632-639.

7 A. Zitolo, V. Goellner, V. Armel, M. T. Sougrati, T. Mineva, L. Stievano, E. Fonda and F. Jaouen, *Nat. Mater.*, 2015, **14**, 937-942.

8 M. Lefèvre, E. Proietti, F. Jaouen and J.-P. Dodelet, *Science*, 2009, **324**, 71-74.

9 M. Kim, H. S. Kim, S. J. Yoo, W. C. Yoo and Y.-E. Sung, *J. Mater. Chem. A*, 2017, **5**, 4199-4206.

10 Z.-L. Wang, D. Xu, H.-X. Zhong, J. Wang, F.-L. Meng and X.-B. Zhang, *Sci. Adv.*, 2015, **356**, 1-9.

11 H. W. Liang, W. Wei, Z. S. Wu, X. Feng and K. Mullen, *J. Am. Chem. Soc.*, 2013, **135**, 16002-16005.

12 J. Xi, Y. Xia, Y. Xu, J. Xiao and S. Wang, *Chem. Commun.*, 2015, **51**, 10479-10482.

13 L. Huo, B. Liu, G. Zhang, R. Si, J. Liu and J. Zhang, *J. Mater. Chem. A*, 2017, **5**, 4868-4878.

14 Y. Qin, L. Chao, J. J. He, Y. Liu, F. Chu, J. Cao, Y. Kong and Y. Tao, *J. Power Sources*, 2016, **335**, 31-37.

15 A. Serov, K. Artyushkova, E. Niangar, C. Wang, N. Dale, F. Jaouen, M.-T. Sougrati, Q. Jia, S. Mukerjee and P. Atanassov, *Nano Energy*, 2015, **16**, 293-300.

16 U. I. Kramm, J. Herranz, N. Larouche, T. M. Arruda, M. Lefevre, F. Jaouen, P. Bogdanoff, S. Fiechter, I. Abs-Wurmbach, S. Mukerjee and J. P. Dodelet, *Phys. Chem. Chem. Phys.*, 2012, **14**, 11673-11688.

17 Y. Jiang, L. Yang, T. Sun, J. Zhao, Z. Lyu, O. Zhuo, X. Wang, Q. Wu, J. Ma and Z. Hu, *ACS Catal.*, 2015, **5**, 6707-6712.

18 D. Lu, D. Wu, J. Jin and L. Chen, *Electrochim. Acta*, 2016, **215**, 66-71.

19 R.-S. Zhong, Y.-H. Qin, D.-F. Niu, J.-W. Tian, X.-S. Zhang, X.-G. Zhou, S.-G. Sun and W.-K. Yuan, *J. Power Sources*, 2013, **225**, 192-199.

20 J. Xiao, Y. Xu, Y. Xia, J. Xi and S. Wang, *Nano Energy*, 2016, **24**, 121-129.

21 Y. Li, H. Zhang, P. Liu, Y. Wang, H. Yang, Y. Li and H. Zhao, *Electrochem. Commun.*, 2015, **51**, 6-10.

22 T.-D. Nguyen, K. E. Shopsowitz and M. J. MacLachlan, *J. Mater. Chem. A*, 2014, **2**, 5915.

23 U. I. Kramm, M. Lefevre, N. Larouche, D. Schmeisser and J. P. Dodelet, *J. Am. Chem. Soc.*, 2014, **136**, 978-985.

24 J. Li, S. Ghoshal, W. Liang, M.-T. Sougrati, F. Jaouen, B. Halevi, S. McKinney, G. McCool, C. Ma, X. Yuan, Z.-F. Ma, S. Mukerjee and Q. Jia, *Energy Environ. Sci.*, 2016, **9**, 2418-2432.

25 N. R. Sahraie, U. I. Kramm, J. Steinberg, Y. Zhang, A. Thomas, T. Reier, J. P. Paraknowitsch and P. Strasser, *Nat. Commun.*, 2015, **6**, 8618.

26 A. Morozan, M. T. Sougrati, V. Goellner, D. Jones, L. Stievano and F. Jaouen, *Electrochim. Acta*, 2014, **119**, 192-205.

27 Y. J. Sa, D. J. Seo, J. Woo, J. T. Lim, J. Y. Cheon, S. Y. Yang, J. M. Lee, D. Kang, T. J. Shin, H. S. Shin, H. Y. Jeong, C. S. Kim, M. G. Kim, T. Y. Kim and S. H. Joo, *J. Am. Chem. Soc.*, 2016, **138**, 15046-15056.

28 L. Birry, J. H. Zagal and J.-P. Dodelet, *Electrochem. Commun.*, 2010, **12**, 628-631.

29 J. Wei, Y. Hu, Z. Wu, Y. Liang, S. Leong, B. Kong, X. Zhang, D. Zhao, G. P. Simon and H. Wang, J. Mater. Chem. A, 2015, **3**, 16867-16873.

30 G. Yang, W. Choi, X. Pu and C. Yu, Energy Environ. Sci., 2015, **8**, 1799-1807.

DOI: 10.1039/C7TA05035F

TOC

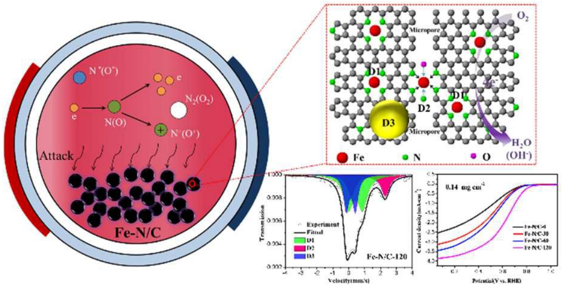

Plasma etching removed less stable carbons and exposed the active sites in Fe-N/C catalysts and resulted in excellent performances towards oxygen reduction reaction in both acidic and alkaline media.